Springer

Acta Mechanica Sinica

CrossMark click for updates

• RESEARCH PAPER •

Acta Mech. Sin., Vol. 41, 624016 (2025)
https://doi.org/10.1007/s10409-024-24016-x

# Assessment of bone strength and fracture behavior of degenerative vertebrae through quantifying morphology and density distribution

Meng Zhang[1,2], He Gong[2,3*], and Ming Zhang[4]

[1] *College of Biomedical Engineering, Taiyuan University of Technology, Taiyuan 030024, China;*
[2] *Department of Engineering Mechanics, Nanling Campus, Jilin University, Changchun 130025, China;*
[3] *School of Biological Science and Medical Engineering, Beihang University, Beijing 100191, China;*
[4] *Department of Biomedical Engineering, The Hong Kong Polytechnic University, Hong Kong, China*

Received April 15, 2024; accepted May 27, 2024; published online August 15, 2024

Lumbar degeneration leads to changes in geometry and density distribution of vertebrae, which could further influence the mechanical property and behavior. This study aimed to quantitatively describe the variations in shape and density distribution for degenerated vertebrae by statistical models, and utilized the specific statistical shape model (SSM)/statistical appearance model (SAM) modes to assess compressive strength and fracture behavior. Highly detailed SSM and SAM were developed based on the 75 L1 vertebrae of elderly men, and their variations in shape and density distribution were quantified with principal component (PC) modes. All vertebrae were classified into mild ($n$ = 22), moderate ($n$ = 29), and severe ($n$ = 24) groups according to the overall degree of degeneration. Quantitative computed tomography-based finite element analysis was used to calculate compressive strength for each L1 vertebra, and the associations between compressive strength and PC modes were evaluated by multivariable linear regression (MLR). Moreover, the distributions of equivalent plastic strain (PEEQ) for the vertebrae assigned with the first modes of SSM and SAM at mean ± 3SD were investigated. The Leave-One-Out analysis showed that our SSM and SAM had good performance, with mean absolute errors of 0.335±0.084 mm and 64.610±26.620 mg/cm$^3$, respectively. A reasonable accuracy of bone strength prediction was achieved by using four PC modes (SSM 1, SAM 1, SAM 4, and SAM 5) to construct the MLR model. Furthermore, the PEEQ values were more sensitive to degeneration-related variations of density distribution than those of morphology. The density variations may change the deformity type (compression deformity or wedge deformity), which further affects the fracture pattern. Statistical models can identify the morphology and density variations in degenerative vertebrae, and the SSM/SAM modes could be used to assess compressive strength and fracture behavior. The above findings have implications for assisting clinicians in pathological diagnosis, fracture risk assessment, implant design, and preoperative planning.

**Statistical shape model, Statistical appearance model, Lumbar degeneration, Compressive strength, Fracture behavior**

**Citation:** M. Zhang, H. Gong, and M. Zhang, Assessment of bone strength and fracture behavior of degenerative vertebrae through quantifying morphology and density distribution, Acta Mech. Sin. 41, 624016 (2025), https://doi.org/10.1007/s10409-024-24016-x

## 1. Introduction

As one of the most important bone structures, lumbar spine is subject to large compressive loads and repetitive motions [1]. Due to this load-bearing characteristic, the lumbar vertebrae are at high risk of degenerative changes [2]. Lumbar degeneration is a particularly common condition among aging adults, and its major complication is low back pain. It was estimated that more than 40% of people aged over 60 suffered from degeneration-related low back pain [3]. Early diagnosis and intervention of degeneration is the most effective way to prevent and relieve low back pain. In general, degeneration could lead to changes in geometry and density distribution of vertebrae [4,5], which may further influence bone mechanical property and behavior. Therefore, it is necessary to quantify the variations of shape and

*Corresponding author. E-mail address: bmegonghe@buaa.edu.cn (He Gong)
Executive Editor: Jizeng Wang

density distribution in vertebrae among the elderly population to improve understanding of the relevant mechanisms of lumbar degeneration, which could assist clinicians in pathological diagnosis and disease treatment.

In previous studies, the shape variation in human vertebrae was quantified by direct measurements on cadaveric specimens [6], manual measurements from computed tomography (CT) images [7], and analysis of three-dimensional (3D) reconstructed models [8]. Furthermore, the regional measurement of bone mineral density (BMD) was usually used to quantify the variation of density distribution in vertebrae. To investigate the variation of density distribution in L1 vertebral bodies, 36 regions in vertebral body (three layers with twelve regions) were defined in our previous study, and the corresponding regional densities of 80 subjects were statistically analyzed [9]. In a recent study, the variation of density distribution in 148 L3 vertebral bodies was characterized by using seven regional densities (anterior, posterior, superior, mid-transverse, inferior, central, and outer regions) [10]. However, the above methods entailed heavy manual effort, which could be tedious, time-consuming, and expert-driven [11]. In addition, these quantitative methods are implemented at a subject-specific level by measuring limited geometric and density features, thus they are unable to capture all detailed variations within the study population [12].

To address the above issues, the statistical shape model (SSM) and statistical appearance model (SAM) were proposed to systematically quantify and analyze the variations of shape and density distribution [13]. SSM and SAM are regarded as promising tools, because they could capture all of the available information from radiology images [14,15]. The key concept behind statistical modeling is to perform principal component analysis (PCA) on contour landmarks and the sampled densities within the contours to extract the independent modes (principal components) of variation [16,17]. Therefore, the shape and density distribution of bones could be described by a linear combination of principal components in details. Recently, the bone research community has realized that SSM and SAM have great potential in many orthopedic applications, especially in implant design [18,19] and fracture risk prediction [20-22].

For the lumbar spine, studies were focused on the use of statistical models to describe the morphology variations in the vertebrae, functional spinal units, and entire spine [4], to identify the significant differences in anatomical shapes between men and women [23], and to develop an automatic segmentation pipeline for patient-specific biomechanical models [24]. To the best of our knowledge, it is not yet well understood about the variations of shape and density distribution in degenerated vertebrae, and little is known about the influences of these variations on bone strength and fracture behavior.

Accordingly, the purposes of this study were: (1) to develop detailed statistical models to quantitatively describe the variations of the shape and density distribution in degenerated vertebrae, (2) to compare the differences in shape and density distribution among the vertebrae with different degenerative states, (3) to investigate the associations between compressive strength and principal component (PC) modes identified by statistical models, and (4) to explore influences of major PC modes on fracture risk and fracture pattern.

## 2. Materials and methods

### 2.1 Study participants and QCT imaging

In this study, 75 subjects (age 71±4.1 years) were included from the Osteoporotic Fractures in Men (MrOS) cohort in Hong Kong part, which is a cross-sectional study investigating the risk factors of osteoporosis fractures in elderly men (age $\geq$ 65 years) [25]. All participants were classified into mild ($n$ = 22), moderate ($n$ = 29), and severe ($n$ = 24) groups according to the overall degree of L1 vertebral degeneration identified from quantitative CT (QCT) images in lateral and anteroposterior views by means of the grading system [26], which covers the three main radiographic signs (i.e., height loss, osteophyte formation, and diffuse sclerosis). Differences in demographic characteristics of study participants in the three degenerative groups were compared using one-way ANOVA. Age, weight, and height showed no significant differences among the groups ($p > 0.05$) (Table 1).

After obtaining written informed consent from participants, the QCT scans of their lumbar vertebrae were performed by the standard protocol. Scan parameters were as follows: 120 kVp, 205.95 mA, 0.9375 × 0.9375 mm/pixel resolution, 1.25 mm slice thickness, 48 cm field of view, and 512×512 matrix in spiral reconstruction mode (GE Medical Systems/LightSpeed 16, Wakesha, WI, USA). To convert CT grayscale value from Hounsfield units (HU) to equivalent BMD, a three-sample calibration phantom (Image Analysis, Columbia, KY, USA) was scanned with participants (hydroxyapatite density: 0, 75, and 150 mg/cm$^3$).

### 2.2 Development of SSM and SAM for L1 vertebra

To quantitatively describe the independent variations of the

**Table 1** Demographic characteristics of the study participants in different degenerative groups (data are presented as mean (standard deviation))

| Characteristics | Mild ($n$ = 22) | Moderate ($n$ = 29) | Severe ($n$ = 24) |
|---|---|---|---|
| Age (years) | 69.50 (3.07) | 71.24 (3.59) | 70.75 (5.24) |
| Weight (kg) | 58.87 (7.65) | 59.52 (7.27) | 61.60 (7.16) |
| Height (cm) | 163.61 (6.47) | 162.36 (5.36) | 162.23 (4.96) |

shape and bone density distribution in the L1 vertebra from elderly men, the QCT images of all subjects were used to develop the SSM and SAM. The modeling process was performed while blinded to the degeneration state of each L1 vertebra to eliminate potential bias.

The detailed procedures for developing SSM and SAM are shown in Fig. 1. To obtain the 3D bone geometry from QCT scans for developing SSM, each L1 vertebra was semi-automatically segmented by using Stradview (University of Cambridge Department of Engineering, Cambridge, UK). Afterward, the similarity transformation and thin plate spline (TPS) registration algorithm were used to nonrigidly align each vertebra surface to a canonical surface with 8329 vertices in wxRegSurf (University of Cambridge Department of Engineering, Cambridge, UK) [27]. Following the Procrustes analysis, the effects of translation, rotation, and scaling were removed [28], and the vertex coordinates of all vertebrae were standardized. PCA was then applied on the vertex matrix to identify a number of orthogonal modes with PC scores that could describe the shape variation of 75 vertebrae [29].

The first step in the development of SAM is obtaining the template vertebra surface by averaging vertex coordinates for all vertebrae. A template mesh was generated based on the average vertebral surface, which consisted of 81952 tetrahedral elements and 18104 nodes. To establish the mesh correspondence among different vertebrae, the template mesh was morphed to match the target vertebra through displacement vectors calculated between corresponding vertices on the template and individual vertebral surfaces (HyperMesh 13.0; Altair Engineering, Troy, USA). Subsequently, grayscale values were mapped from the QCT scans to the morphed finite element meshes by using Mimics 17.0 (Materialise, Leuven, Belgium). Following the relationship between BMD and grayscale value, the spatial density distribution of each vertebra was obtained. Similar to the SSM, the SAM was developed by performing PCA on the BMD values assigned to the tetrahedral elements. The main modes with PC scores were obtained to describe the variation in the density distribution of 75 vertebrae.

The generalization capabilities of the SSM and SAM were evaluated by using the leave-one-out (LOO) analysis, which was normally used for validating the ability of the statistical model to reconstruct an unknown or previously unseen subject [30,31]. In this analysis, one vertebra was removed in turn from 75 samples and used as the left-out vertebra. PCA was then applied to the vertex matrix/BMD values of the remained vertebrae to develop a statistical model. The shape and density distribution of each left-out vertebra were reconstructed by the statistical models. To quantify the accuracy of shape reconstruction, the mean absolute error between vertex coordinates of the left-out vertebra and the reconstructed vertebra ($MAE_{SSM}$) was computed. Similarly, the mean absolute error between BMD values of meshes in the left-out vertebra and the reconstructed vertebra ($MAE_{SAM}$) was computed to estimate the reconstruction accuracy of spatial density distribution.

### 2.3 Estimation of compressive strength of the L1 vertebra

The compressive strength of the L1 vertebra in our study was estimated following the QCT-based finite element analysis (QCT/FEA) processes similar to those described elsewhere [32,33]. Of note, the QCT/FEA model of each L1 vertebra was developed according to the original QCT images, and not the template vertebra with mapped BMD. Specifically, the QCT images were rotated into a standard orientation and then resliced to 1 mm isotropic resolution. L1 vertebra was segmented from the consecutive QCT images. Each QCT voxel was converted directly to a voxel-type mesh (1 mm × 1 mm × 1 mm, cube-shaped, eight-noded linear brick element) and assigned elastic and plastic material properties based on the proposed empirical relationships to BMD [34]. A total of 150 kinds of material

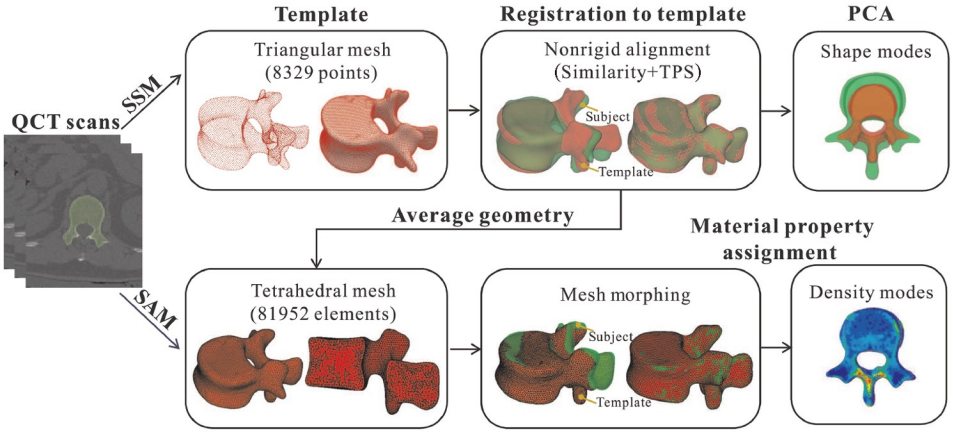


**Figure 1** Schematic description about the procedures of developing SSM and SAM.

properties were set [9]. To simulate the uniaxial compression configuration commonly used in the mechanical test, the superior and inferior ends of each vertebral body were embedded into two 3 mm layers of polymethylmethacrylate (PMMA) [35]. The material properties of PMMA were set as isotropic linear elastic ($E$ = 2500 MPa, $\mu$ = 0.3) [36]. All nodes on the inferior PMMA layer were fixed, and a prescribed displacement equivalent to 2% longitudinal compressive strain was applied to the superior PMMA layer. The compressive strength of the L1 vertebra was defined as the total reaction force generated at 2% strain [33]. The calculated strengths were validated by comparing with the results from previous studies, which were described in the Discussion section.

### 2.4 Statistical analyses

The differences in scores of the SSM and SAM modes between the degenerative groups were compared by one-way ANOVA with LSD post-hoc tests in SPSS 19.0 (IBM Inc., Chicago, USA). To investigate the associations between compressive strength of L1 vertebra and PC modes identified by SSM and SAM, multivariable linear regression (MLR) models were constructed with PC modes as the independent variables and the compressive strength as the dependent variable. To obtain the optimized predictive model and avoid over-fitting, only the first 10 modes of SSM and the first 10 SAM modes were included in the MLR models [15]. The model selection was based on Bayes information criterion. To quantify the performance of MLR models, the root mean squared error (RMSE) and the adjusted coefficient of determination $R^2$ ($R^2_{\text{adj}}$) were used. Three-fold cross-validation analyses repeated 10 times were used to compare the predictive ability of the obtained MLR models [37]. The 30 estimates of RMSE and $R^2_{\text{adj}}$ for each MLR model were averaged and their 95% confidence intervals (CI) were calculated. Pairwise $t$-tests were then used to compare the performance metrics (i.e., RMSE and $R^2_{\text{adj}}$) across the predictive models, with the Holm method for adjusting $p$-values. The MLR analysis was performed in R v4.0.3 (R Foundation for Statistical Computing, Vienna, Austria). The level of significance for all statistical analyses was set to 5%.

## 3. Results

### 3.1 Geometrical comparisons of vertebrae in different degenerative groups

The typical geometries of L1 vertebrae in the three degenerative groups (i.e., subjects #17, #40, and #52) are shown in Fig. 2(a). To quantitatively describe the shape variations with increasing severity of degeneration, the differences of vertex coordinates in the average vertebrae for the mild, moderate, and severe groups (mild vs. moderate groups and moderate vs. severe groups) were calculated and illustrated in Fig. 2(b). For the degenerative process from mild to moderate grades, the shape changes of L1 vertebra were uniform. The shape variations in vertebral body were dominated by the decreased height and increased width, whereas it was found that the height of spinous process was visibly increased in the posterior elements, with the maximum deformation of 1.87 mm. The spinal nerves may be easily impinged and irritated because of hypertrophy in the tips of the spinous process, which could lead to acute or chronic low back pain.

For the degenerative process from moderate to severe grades, the shape changes in the vertebral body were non-uniform, and the predominant variations were caused by the growth of bone spurs (also known as osteophytes) at the anterolateral edges of the vertebral body, with the maximum deformation of 2.50 mm. Moreover, the decreased length of the transverse process was the most obvious change in the posterior elements. The intertransverse ligaments are interposed between the transverse processes of adjacent vertebrae. Thus, the above shape change may contribute to the overstretching and damage of ligaments, which could eventually lead to the limited movement of the upper lumbar levels (i.e., L1-L2 and L2-L3).

### 3.2 Comparisons of BMD distribution for vertebrae in different degenerative groups

The means and standard deviations of BMD values in the overall vertebra, vertebral body, and posterior elements fordifferent degenerative groups are shown in Fig. 2(c). The BMD value of vertebral body in the severe group was significantly higher than those in mild and moderate groups (233.02±27.38 mg/cm$^3$ vs. 208.00±31.88 mg/cm$^3$ and 214.36±23.44 mg/cm$^3$, respectively; $p < 0.05$). Conversely, there were no significant BMD differences in the overall vertebra and posterior elements among the three degenerative groups ($p > 0.05$). To further compare the spatial density distribution between vertebrae in the severe group and mild/moderate group, the differences between average BMD values of meshes were calculated and depicted in Fig. 2(d), with higher BMD in the severe group having a positive value. For the comparison of BMD distribution between the mild and severe groups, severely degenerated vertebrae had lower densities in the posterior region of spinal foramen, and higher densities at the anterolateral edges of the vertebral body and the tips of the spinous process, reaching a maximum difference with the value of 261.10 mg/cm$^3$. Similarly, the BMD values at the anteroinferior edges of the vertebral body and the tips of the spinous process tended to

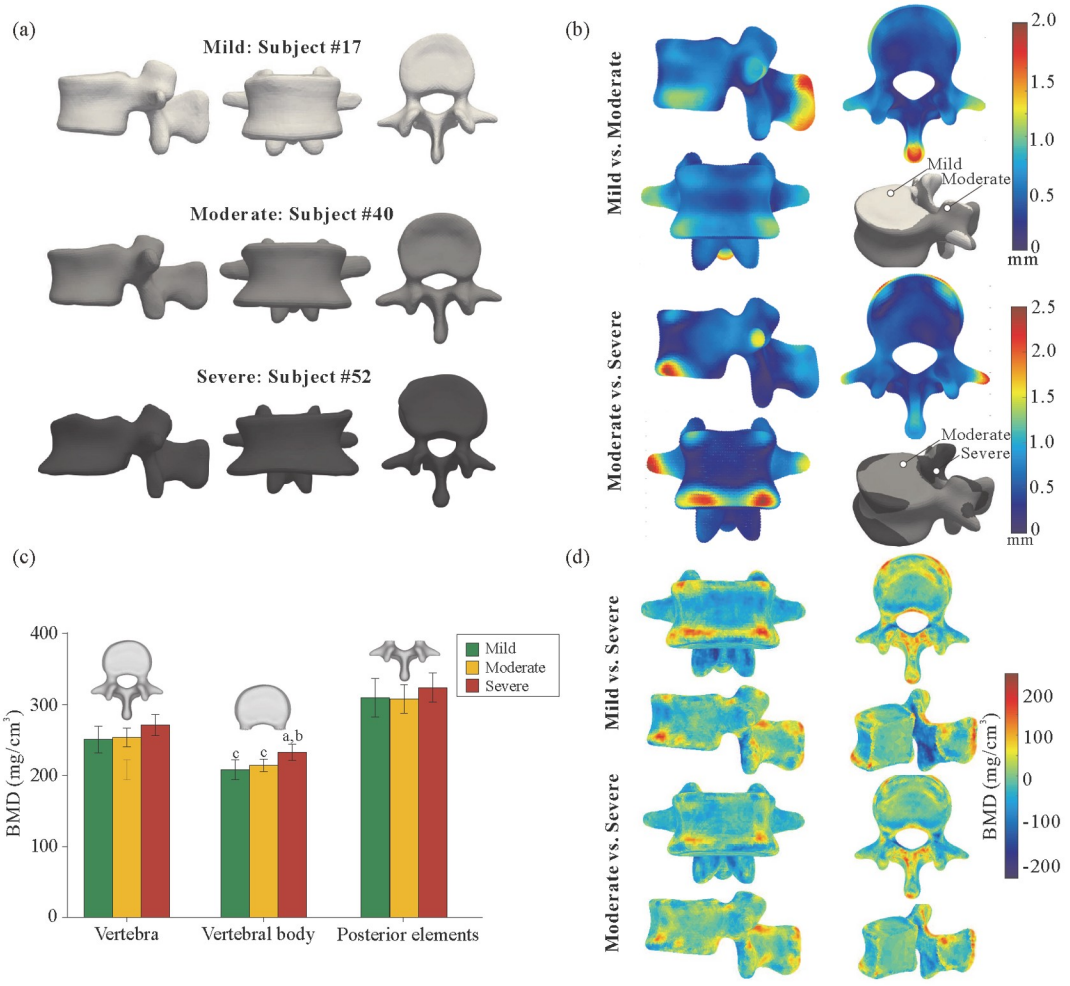


**Figure 2** Comparisons of geometry and BMD distribution for L1 vertebrae with different degeneration states. (a) The typical geometries of vertebrae in the three degenerative groups. Subjects #17, #40, and #52 were from the mild, moderate, and severe groups, respectively. (b) The differences of the vertex coordinates in the average vertebrae for the mild, moderate, and severe groups (mild vs. moderate groups and moderate vs. severe groups). (c) The means and standard deviations of BMD values in the overall vertebra, vertebral body, and posterior elements for different degenerative groups. [a] Statistically different from the mild group ($p < 0.05$); [b] Statistically different from the moderate group ($p < 0.05$); [c] Statistically different from the severe group ($p < 0.05$). (d) The differences of spatial density distribution between vertebrae in the severe group and mild/moderate group.

be higher in the severe group than the moderate group, reaching a maximum difference with the value of 203.40 mg/cm$^3$. Furthermore, vertebrae in the severe group had slightly lower densities in the posterior region of spinal foramen compared to moderately degenerated vertebrae.

### 3.3 SSM analysis

The SSM identified 74 independent modes to describe the total shape variation of the L1 vertebra. The first 37 modes cumulatively explained more than 95% of shape variation, in which the first three modes were responsible for 51.2% of the overall variation. The mean shape of 75 vertebrae and the shape variations explained by the first three modes are shown in Fig. 3. As expected, the first mode of SSM (SSM 1) described geometrical scaling, capturing most of the shape variations (34.7%). However, the scaling variation was non-uniform, scalings in mediolateral and anteroposterior directions of vertebra were greater than that in superoinferior direction. The size of vertebral body and the length of transverse process were identified by the shape mode 2 (SSM 2), which accounted for 9.7% variability. Additionally, the third mode of SSM (SSM 3) comprised 6.8% of the total anatomical variation and it corresponded to pedicle transverse angle roughly. The LOO analysis for the SSM resulted in relatively low $MAE_{SSM}$ (0.335±0.084 mm), which implied that the present SSM could properly describe the shape variation of the L1 vertebra in elder men.

Statistically significant differences were observed in the scores of the fifth and the eleventh modes of SSM (i.e., SSM 5 and SSM 11) among all degenerative groups ($p < 0.05$). SSM 5 related closely to the height of vertebral body (Fig. 3), which explained 3.7% of shape variation. For this mode, the score in the mild group was significantly higher than those

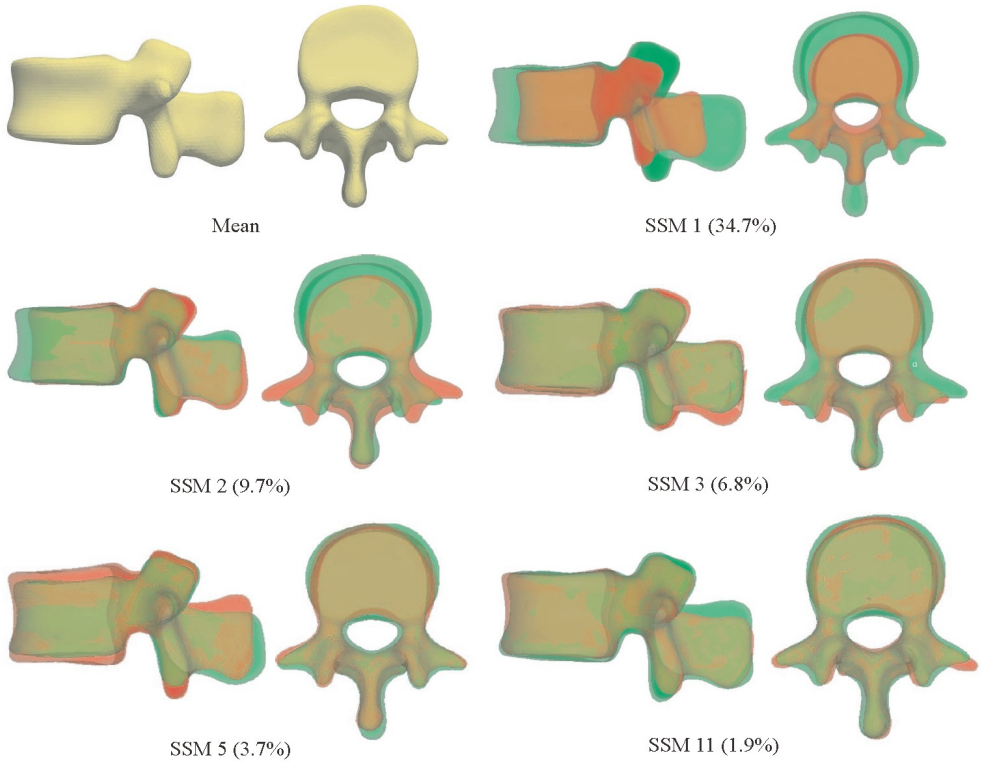


**Figure 3** Mean shape of 75 vertebrae and the shape variations identified by the specific SSM modes (SSM 1, SSM 2, SSM 3, SSM 5, and SSM 11) with indication for the percentage of overall variation. Green is +3SD, red is −3SD.

in the moderate and severe groups ($p < 0.05$), with the values of 0.604±1.120 vs. −0.049±0.710 and −0.495±0.922, respectively (Table 2). Moreover, SSM 11, which captured the height of spinous process and width of vertebral body (Fig. 3), significantly discriminated the severe group and mild/moderate group ($p < 0.05$), with the scores of −0.513 ±0.816 vs. 0.447±0.801 and 0.084±1.106, respectively (Table 2). Accordingly, the degeneration state of individual L1 vertebra could be roughly identified by the score values of SSM 5 and SSM 11. As shown in Fig. 4(a), most of vertebrae in the mild group were distributed in the right-top region of the scatter plot (corresponding to high scores of SSM 5 and SSM 11), whereas the vertebrae in the left-bottom region were mainly from the severe group (corresponding to low scores of SSM 5 and SSM 11).

**Table 2** Score values of SSM 5, SSM 11, SAM 2, SAM 3, and SAM 5 in different degenerative groups (data are presented as mean (standard deviation))

| | Mild ($n$ = 22) | Moderate ($n$ = 29) | Severe ($n$ = 24) |
|---|---|---|---|
| SSM 5 | 0.604 (1.120) [b, c] | −0.049 (0.710) [a] | −0.495 (0.922) [a] |
| SSM 11 | 0.447 (0.801) [c] | 0.084 (1.106) [c] | −0.513 (0.816) [a, b] |
| SAM 2 | 0.516 (0.685) [c] | 0.218 (0.857) [c] | −0.736 (1.008) [a, b] |
| SAM 3 | 0.516 (0.681) [c] | 0.073 (0.759) [c] | −0.562 (1.225) [a, b] |
| SAM 5 | 0.518 (1.305) [b, c] | −0.301 (0.708) [a] | −0.112 (0.817) [a] |

[a] Statistically different from the mild group ($p < 0.05$); [b] Statistically different from the moderate group ($p < 0.05$); [c] Statistically different from the severe group ($p < 0.05$).

### 3.4 SAM analysis

The SAM was less compact than SSM, 63 modes (out of a total of 74 modes) were needed to account for more than 95% of the variation in BMD distribution. The first three modes of SAM accounted for only 27.9% of the variation, and the density variations described by them are visualized in Fig. 5. The first mode of SAM (SAM 1) described the overall change in density, which accounted for 17.5% of the total variation in BMD distribution. The second mode (SAM 2) was primarily associated with the density variation in posterior elements, explaining 6.4% variability. The third mode of SAM (SAM 3) captured 4.0% of the variation and identified the density changes in the vertebral body and posterior region of spinal foramen. From the LOO analysis, the $MAE_{SAM}$ values for the reconstructed BMD distribution of unknown vertebrae were 64.610±26.620 mg/cm$^3$, suggesting a relatively high accuracy of our SAM.

Analysis of the SAM scores for the three degenerative groups showed that statistical differences were only observed for modes 2, 3, and 5 ($p < 0.05$). The SAM 2 and SAM 3 scores in the severe group were negative, and they were significantly lower than those in the mild/moderate group ($p < 0.05$) (Table 2). The fifth mode of SAM (SAM 5) mainly described the variations of BMD distribution in the cortical bone of vertebral body and the spinous process, accounting for 2.7% variability (Fig. 5). The SAM 5 score in

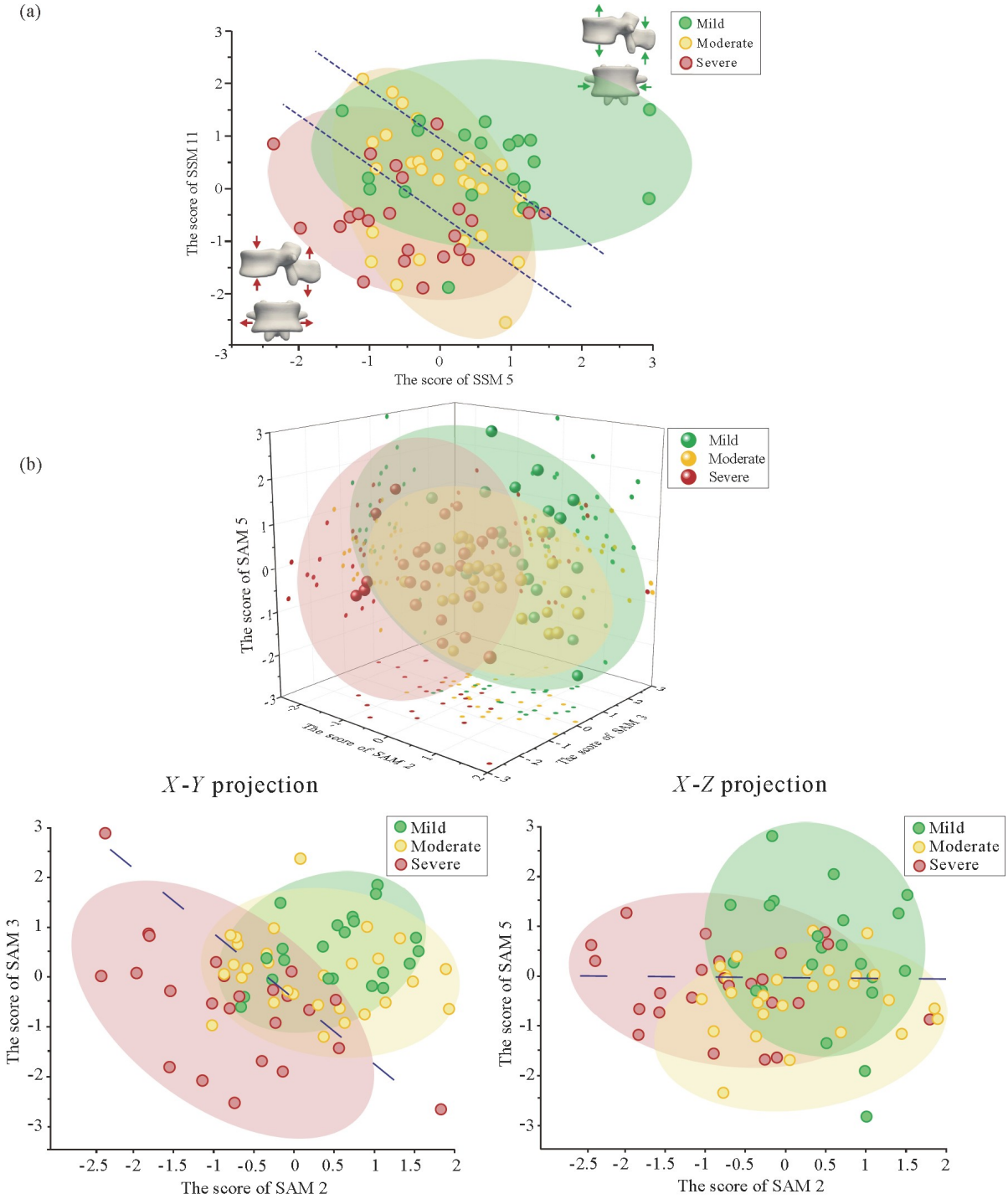


**Figure 4** Scatter plots of the specific SSM and SAM scores for vertebrae with different degeneration states. The blue lines indicate the rough classification boundaries. (a) Scatter plot of SSM 5 vs. SSM 11 scores for vertebrae with different degeneration states. (b) Scatter plot of the SAM 2, SAM 3, and SAM 5 scores for vertebrae with different degeneration states.

the mild group was significantly different from the moderate/severe group (0.518±1.305 vs. −0.301±0.708 and −0.112±0.817, respectively; $p < 0.05$) (Table 2). Accordingly, the degeneration state of individual L1 vertebra could be roughly identified by means of SAM 2, SAM 3, and SAM 5. As shown in Fig. 4(b), SAM 2 and SAM 3 could be used to identify the vertebrae in the severe group, and the vertebrae in the mild and moderate groups could be roughly discriminated through the score of SAM 5, because the directions of the SAM 5 scores in these two groups were generally inverse (positive value for the mild group and negative value for the moderate group).

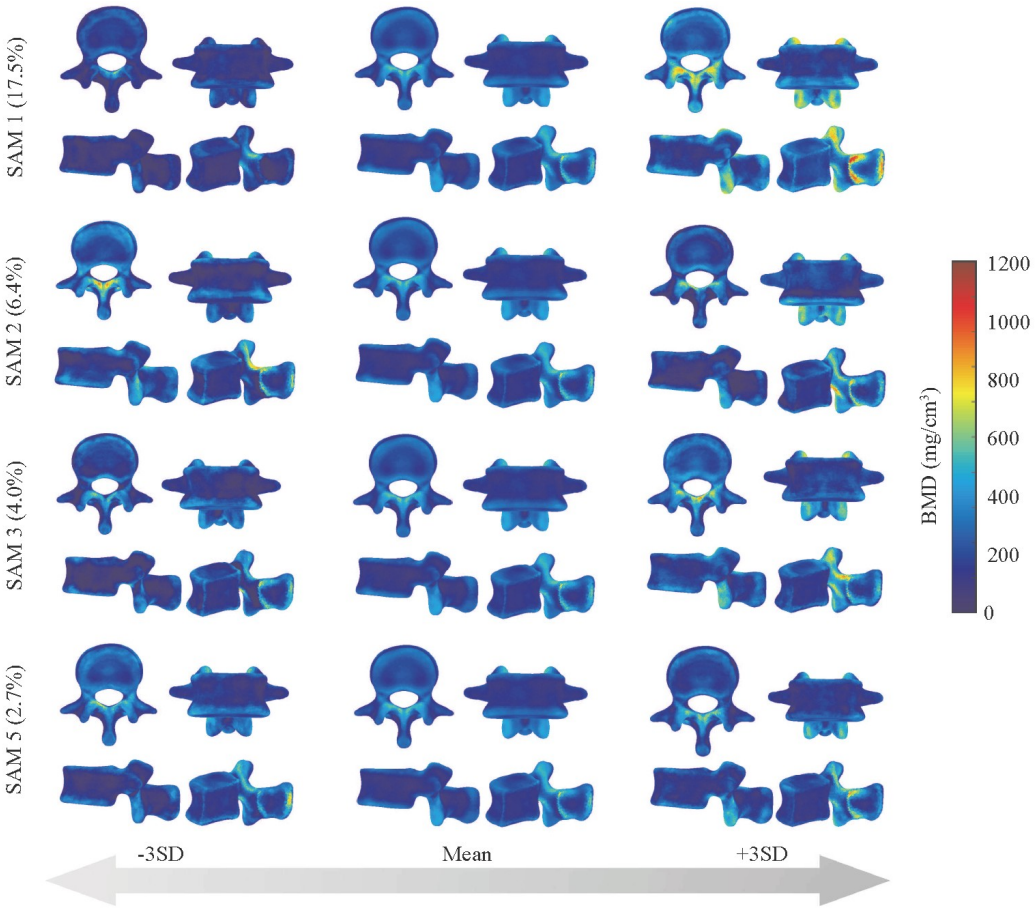


**Figure 5** Variations of BMD distribution explained by the specific SAM modes (SAM 1, SAM 2, SAM 3, and SAM 5) with indication for the percentage of overall variation. Each SAM mode is visualized at mean ± 3SD.

### 3.5 MLR models for compressive strength of L1 vertebra

Five MLR models were constructed to describe the relationships between compressive strength of the L1 vertebra and the first 10 modes of SSM and SAM (Table 3). The performance of MLR models improved with the number of modes included, and the SSM and SAM modes identified from MLR analysis were, in order of importance, SAM 1, SSM 1, SAM 5, SAM 4, and SSM 2. SAM 1 was the most important independent variable, yielding an $R^2_{adj}$ value of 0.658. By adding the SAM 4, SAM 5, and SSM 1 to Model 1 (Model 4), the $R^2_{adj}$ value improved to 0.825 and the RMSE decreased from 931.473 N to 653.887 N. Further inclusion of SSM 2 resulted in a minor increase in the $R^2_{adj}$ value from 0.825 to 0.837 and a minor decrease in the RMSE from 653.887 N to 625.660 N (Model 5).

The predictive abilities of the obtained MLR models were compared using the three-fold cross-validation analysis. As shown in Table 4, the performance of Model 1 was significantly worse than the other models ($p < 0.001$), with the RMSE of 926.945 N and the $R^2_{adj}$ value of 0.654. Models 4 and 5 explained the greatest amount of variation in the compressive strength of L1 vertebra ($R^2_{adj}$ = 0.802 and 0.808, respectively) and had the lowest RMSE among all predictive models (RMSE = 646.143 N and 619.069 N, respectively). Of note, no significant difference was found between the RMSE and $R^2_{adj}$ values of Models 4 and 5 ($p > 0.05$), which implied that the performance of these two models was similar. The RMSE of Models 4 and 5 were significantly lower than those of other models ($p < 0.05$). In addition, the RMSE of Model 2 was significantly higher than that of Model 3 (+7.9%, $p = 0.048$), and the $R^2_{adj}$ of Model 2 was significantly lower than those of Model 4 and Model 5 ($p < 0.05$).

To compare the performances of the MLR model for predicting vertebral strength in different degenerative groups, the relative errors between vertebral strengths obtained from the QCT/FEA model and the MLR model 4 were computed. The mean relative error in the mild group was less than those in the moderate and severe groups (6.77% vs. 8.66% and 8.09%); however, there were no significant differences in the relative errors among the three degenerative groups ($p > 0.05$).

**Table 3** Predictive models for compressive strength of L1 vertebra

| Model | Variables in the model | Unstandardized coefficient $B$ (SE) [a)] | Standardized coefficient $\beta$ | $p$ | $R^2$ | $R^2_{adj}$ | RMSE (N) |
|---|---|---|---|---|---|---|---|
| Model 1 | (Intercept) | 6742.52 (109.02) | – | < 0.001 | 0.663 | 0.658 | 931.473 |
| | SAM 1 | 1315.56 (109.76) | 0.814 | < 0.001 | | | |
| Model 2 | (Intercept) | 6742.52 (89.05) | – | < 0.001 | 0.778 | 0.772 | 755.647 |
| | SAM 1 | 1307.07 (89.66) | 0.809 | < 0.001 | | | |
| | SSM 1 | 548.38 (89.66) | 0.339 | < 0.001 | | | |
| Model 3 | (Intercept) | 6742.52 (83.59) | – | < 0.001 | 0.807 | 0.799 | 704.377 |
| | SAM 1 | 1307.12 (84.17) | 0.809 | < 0.001 | | | |
| | SAM 5 | −275.46 (84.16) | −0.171 | 0.00165 | | | |
| | SSM 1 | 545.43 (84.17) | 0.338 | < 0.001 | | | |
| Model 4 | (Intercept) | 6742.52 (78.15) | – | < 0.001 | 0.834 | 0.825 | 653.887 |
| | SAM 1 | 1306.39 (78.69) | 0.809 | < 0.001 | | | |
| | SAM 4 | −267.78 (79.92) | −0.166 | 0.00130 | | | |
| | SAM 5 | −274.96 (78.69) | −0.170 | < 0.001 | | | |
| | SSM 1 | 592.34 (79.93) | 0.367 | < 0.001 | | | |
| Model 5 | (Intercept) | 6742.52 (75.32) | – | < 0.001 | 0.848 | 0.837 | 625.660 |
| | SAM 1 | 1301.33 (75.86) | 0.805 | < 0.001 | | | |
| | SAM 4 | −249.39 (77.36) | −0.154 | 0.00193 | | | |
| | SAM 5 | −296.31 (76.30) | −0.183 | < 0.001 | | | |
| | SSM 1 | 588.97 (77.04) | 0.365 | < 0.001 | | | |
| | SSM 2 | 193.43 (76.66) | 0.120 | < 0.001 | | | |

a) SE = standard error.

**Table 4** Performance comparisons for different MLR models[a)]

| Model | RMSE (N) (95% CI) | $p$ | | | |
|---|---|---|---|---|---|
| | | vs. Model 2 | vs. Model 3 | vs. Model 4 | vs. Model 5 |
| Model 1 | 926.945 (888.626-965.263) | **< 0.001** | **< 0.001** | **< 0.001** | **< 0.001** |
| Model 2 | 752.664 (728.035-777.293) | – | **0.048** | **< 0.001** | **< 0.001** |
| Model 3 | 697.490 (663.288-731.691) | – | – | **0.049** | **0.003** |
| Model 4 | 646.143 (611.177-681.109) | – | – | – | 0.239 |
| Model 5 | 619.069 (587.269-650.869) | – | – | – | – |
| Model | $R^2_{adj}$ (95% CI) | $p$ | | | |
| | | vs. Model 2 | vs. Model 3 | vs. Model 4 | vs. Model 5 |
| Model 1 | 0.654 (0.631-0.677) | **< 0.001** | **< 0.001** | **< 0.001** | **< 0.001** |
| Model 2 | 0.760 (0.745-0.775) | – | 0.389 | **0.014** | **0.004** |
| Model 3 | 0.781 (0.760-0.801) | – | – | 0.389 | 0.208 |
| Model 4 | 0.802 (0.781-0.822) | – | – | – | 0.665 |
| Model 5 | 0.808 (0.788-0.827) | – | – | – | – |

a) Statistically significant results are shown in bold font.

### 3.6 Effects of shape and density variations on the fracture behavior

SSM 1 and SAM 1 accounted for the largest proportions of shape and density variations, respectively (Figs. 3 and 5). Moreover, the MLR analysis revealed that these two modes are the major determinants of compressive strength (Table 3). Therefore, SSM 1 and SAM 1 were used to explore the effects of degeneration-related shape and density variations on the fracture behavior. Given the well-established correlation between vertebral fracture and regions of high strain [38], distributions of equivalent plastic strain (PEEQ) for the vertebrae assigned with SSM 1 and SAM 1 at mean ± 3SD were investigated. With the increase of SSM 1 and SAM 1 scores, a discernible reduction in the average PEEQ value of vertebra was observed, indicating a corresponding decrease in the risk of bone fracture (Fig. 6). Furthermore, the PEEQ was more sensitive to degeneration-related variations of density distribution than those of morphology. Specifically, with the same shape, an approximate 24% decrease in the average PEEQ value of vertebra occurred when the SAM 1 score transitioned from −3 to 3 (mean ± 3SD); while with the same density distribution, the decrease of PEEQ value was about 9% when the SSM 1 score transitioned from −3

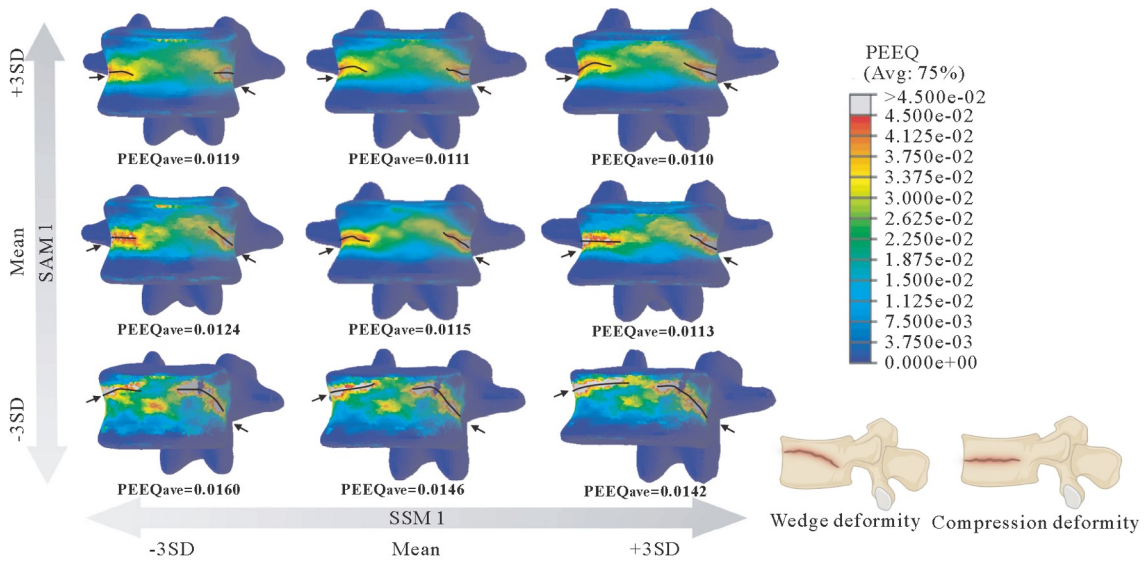


**Figure 6** Distributions of PEEQ for the specific vertebrae at the given shape and density modes (SSM 1 and SAM 1 at mean ± 3SD). Black arrows point to predicted fractures, and $PEEQ_{ave}$ is the average value of PEEQ in the finite element model.

to 3 (mean ± 3SD). Additionally, the degeneration-related variations of density distribution would influence the pattern of vertebral fractures. With the same shape, SAM 1 scores below 0 (mean value) were associated with a tendency towards wedge deformity-induced bone fractures; while positive SAM 1 scores indicated a propensity for compression deformity-induced vertebral fractures. In contrast, shape variation had almost no effect on the fracture pattern.

## 4. Discussion

In this study, highly detailed statistical models (SSM and SAM) were developed based on the 75 L1 vertebrae with different degenerative states (mild, moderate, and severe grades), and their variations in shape and density distribution were quantified with PC modes. The LOO analys is shown that our SSM and SAM had good performance in shape and density reconstructions for unknown vertebrae ($MAE_{SSM}$ = 0.335±0.084 mm, $MAE_{SAM}$ = 64.610±26.620 mg/cm$^3$). There were significant differences in the scores of specific modes (SSM 5, SSM 11, SAM 2, SAM 3, and SAM 5) among the three degenerative groups, which could be used to roughly discriminate degeneration grade. The associations between compressive strength and PC modes identified by SSM and SAM were investigated by MLR analysis. A reasonable accuracy of bone strength prediction ($R^2_{adj}$ = 0.825, RMSE = 653.887 N) was achieved by using SSM 1, SAM 1, SAM 4, and SAM 5 to construct the MLR model. The PEEQ values (high value indicating high fracture risk) were more sensitive to degeneration-related variations of density distribution than those of morphology. Moreover, the density variations may change the deformity type, which further influences the fracture pattern. These findings have implications for assessing fracture risk, assisting clinicians in pathological diagnosis, as well as guiding implant design and preoperative planning.

In our study, the compressive strengths of vertebrae were calculated by the noninvasive method (QCT/FEA). To ensure the accuracy and validity of strength assessment, our QCT/FEA models of L1 vertebra were constructed following the standard procedures [33]. For the 75 vertebrae in this study, the compressive strengths were 6742.52±1615.57 N, ranging from 3981.01 N to 9992.60 N, which were consistent with those reported from the previous studies for the male vertebrae with matched age (≥ 65 years) [9,33]. Moreover, the fracture sites of 75 vertebral bodies were defined as the point that reached the maximum PEEQ at the QCT/FEA-computed vertebral strength, and most of them were located at the regions in the middle layer. These fracture sites have been shown to agree with the subsequent fracture locations [9,34]. Taken together, the QCT/FEA models in our study were reliable and can be used to assess bone strength and PEEQ. In clinics, BMD is currently considered the standard surrogate of bone strength to diagnose osteoporosis and assess the related fracture risk. For the spine, the recommended $BMD_{QCT}$ thresholds for osteoporosis and low bone mass correspond to 80 mg/cm$^3$ and 120 mg/cm$^3$, respectively [39]. In accordance with the linear regression between vertebral strength and $BMD_{QCT}$ of men, the strength interventional thresholds—"fragile bone strength" corresponding to osteoporosis and "low bone strength" corresponding to low bone mass—were defined as 6500 N and 8500 N, respectively. Moreover, the probability of vertebral fracture could be assessed through the well-estab-

lished logistic regression models from a previous study [33], in which vertebral strength/$BMD_{QCT}$ and age were considered as predictors. On the basis of the average age and vertebral strength of the subjects in this study, we estimated that the risk of lumbar vertebral fracture in elderly men would be 10%-15%, which was slightly higher than the value estimated from the $BMD_{QCT}$.

Our study showed that the shape and density distribution of L1 vertebra changed with degeneration progresses. It should be noted that degeneration may also affect bone strength. To investigate the influence of degeneration on bone strength of L1 vertebra, the compressive strengths in different degenerative groups were compared. In particular, the compressive strength in the severe group was significantly higher than those in mild and moderate groups (7453.51±1707.87 N vs. 6138.72±1673.41 N and 6612.16±1290.16 N, respectively; $p < 0.05$). The reason for the above results might be that the degeneration alters the load transfer in vertebra, shifting loads from the weaker anterior region (with lower density) to the stronger posterior region (with higher density) [2]. Prior measurements have shown that for the erect spinal posture, the load applied to the anterior region of vertebra decreases with age [40]. Another reason is that the osteophyte growing in the degenerative process may increase the density heterogeneity. In general, the vertebra with greater heterogeneity in density exhibits higher strength [40].

In addition to bone strength, the stress distribution within vertebra may also be influenced by degeneration. Figure 7 shows the distributions of von Mises stress for the specific vertebrae in different degenerative groups (i.e., subjects #5, #23, and #57). The compressive strengths of these three vertebrae were similar, with values of 5726.01 N, 5752.89 N, and 5774.67 N, respectively. However, their distributions of von Mises stress at the same compressive strains were different. During the compressive deformation, the variations of stress distribution were relatively uniform in the mildly and moderately degenerated vertebrae. In comparison, for the severely degenerated vertebra, more regions with high stresses were found at the vertebral rim. Severe osteophytes on the vertebral body mainly accounted for the non-uniform stress distribution. As degeneration progresses, a greater proportion of the applied loads would be transferred to the outer regions of the vertebral body. This non-uniform load distribution might trigger bone remodeling and lead to bone resorption in the central region [40], which could increase the fracture risk. The above findings indicated that for the vertebrae with similar bone strengths, the severely degenerated subjects may be at higher risk of fracture. Therefore, besides bone strength, the degeneration state also should be considered in the clinical assessment of fracture risk.

Our results suggested some strategies for orthopedic implant design, selection, and placement, as well as surgical planning. Quantification of shape variation for degenerated vertebra is important for pathology-specific implant design since the shape of host bone tissue affects implant sizing and stability [4]. Significant differences in the scores of SSM 5 and SSM 11 among the three degenerative groups indicated that severely degenerated vertebrae have lower vertebral body height, also manifesting as increase in vertebral body width (Table 2 and Fig. 2(b)). This finding suggested that intervertebral implants (such as interbody fusion devices) should be designed to accommodate degeneration-related

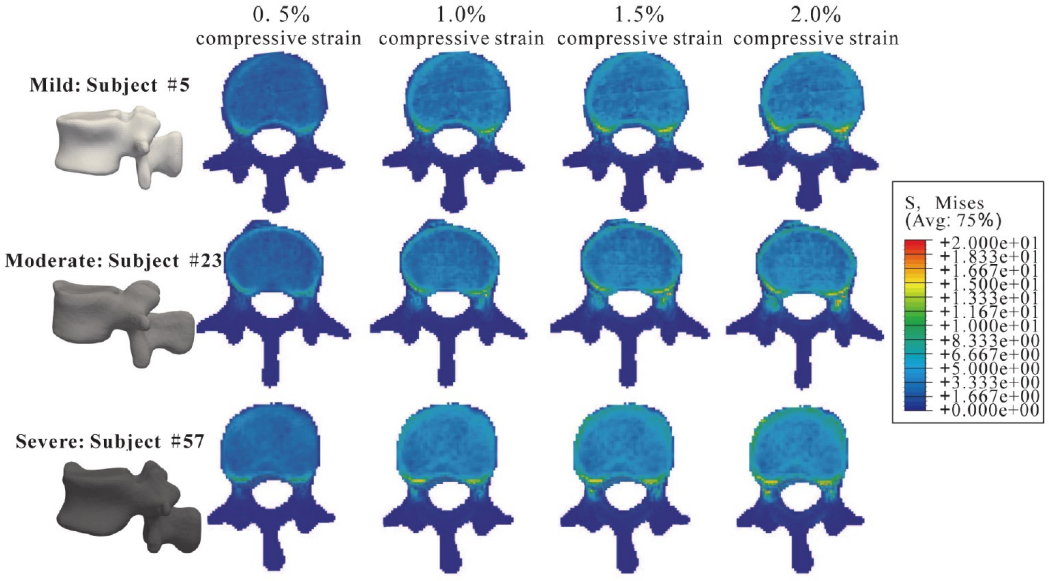


**Figure 7** Distributions of von Mises stress for the specific vertebrae at the given compressive strains. Subjects #5, #23, and #57 were from the mild, moderate, and severe groups, respectively.

shape variations. Moreover, fully understanding the density distribution of vertebra could support decisions related to prosthetic fixation, including selections of optimal placement and trajectory for the insertion [2]. This study showed significantly different density distributions in the posterior elements (captured by SAM 2) for the vertebrae in the severe group and other two groups (mild and moderate groups), and this finding suggested that for the severely degenerated vertebrae, pedicle screws for lumbar fusion should be fixed slightly close to the proximal regions of pedicle, since relatively high densities were observed in these regions (Table 2 and Fig. 2(d)). Considering the preoperative pathological condition (degenerative changes) in the design and positioning of spinal implants could reduce micromotion, increase mechanical stability, and improve patient outcomes.

In this study, five predictive variables of compressive strength (SSM 1, SSM 2, SAM 1, SAM 4, and SAM 5) were identified by the MLR analysis, and the results showed that the global density distribution (SAM 1) is the primary determinant of compressive strength for vertebra, and the overall size (SSM 1) is the secondary factor. These two predictors could explain a moderate amount of variation in compressive strength ($R^2_{adj} = 0.772$) (Table 3). Similar to the current finding, a recent study also demonstrated that the PC modes describing the global density distribution and geometry of femoral neck were important variables for femoral neck strength prediction [15]. Generally, increasing the number of predictive variables improved the performance in the MLR models [15], whereas the increased computational complexity may hamper their application in clinical practice. To select an appropriate predictive model of bone strength, predictive abilities of the obtained MLR models were compared using performance metrics ($R^2_{adj}$ and RMSE). Our results suggested that a reasonable level of performance ($R^2_{adj} = 0.825$, RMSE = 653.887 N) could be achieved by using 3 SAM modes (SAM 1, SAM 4, and SAM 5) and SSM 1 as independent variables (Table 3), and the performances of this MLR model for predicting bone strengths of vertebrae with different degenerative states were similar.

To better understand the respective influence of each shape/density mode selected by MLR analysis on the compressive strength of L1 vertebra, a synthetically generating method, as described in details elsewhere [15], was used to quantify their relative contributions to bone strength. For exploring the influence of shape (SSM 1 and SSM 2), the finite element models with mean shape of 75 vertebrae and the shape at ±1, ±2, and ±3 standard deviations of corresponding shape modes were developed, and the mean spatial density distribution was assigned to all models. Similarly, to explore the influence of bone density distribution (SAM 1, SAM 4, and SAM 5), the mean density distribution of 75 vertebrae and the bone densities at ±1, ±2, and ±3 standard deviations of corresponding density modes were calculated and assigned to the finite element models with the mean vertebra shape. For the independent analyses of shape modes, SSM 1 exhibited a moderate influence on compressive strength, with the range of 4942.49 N to 8302.13 N (Fig. 8(a)). In comparison, SSM 2 had only a negligible influence, ranging from 5765.82 N to 7009.73 N (Fig. 8(a)). It may explain why the MLR model was not sensitive to the absence of SSM 2 (Tables 3 and 4). For the independent analyses of density modes, as shown in Fig. 8(b), SAM 1 had a substantial effect on bone strength, with the widest range varying from 2798.73 N to 9886.59 N. Although SAM 4 accounted for just 3.4% of the variability, it was found to have a moderate influence on bone strength (ranging from 5608.32 N to 7254.09 N). The relative contribution of SAM 5 to bone strength was comparable to SAM 4, and it may be due to the similar percentages of variability explained by them (3.4% and 2.7%, respectively). From the

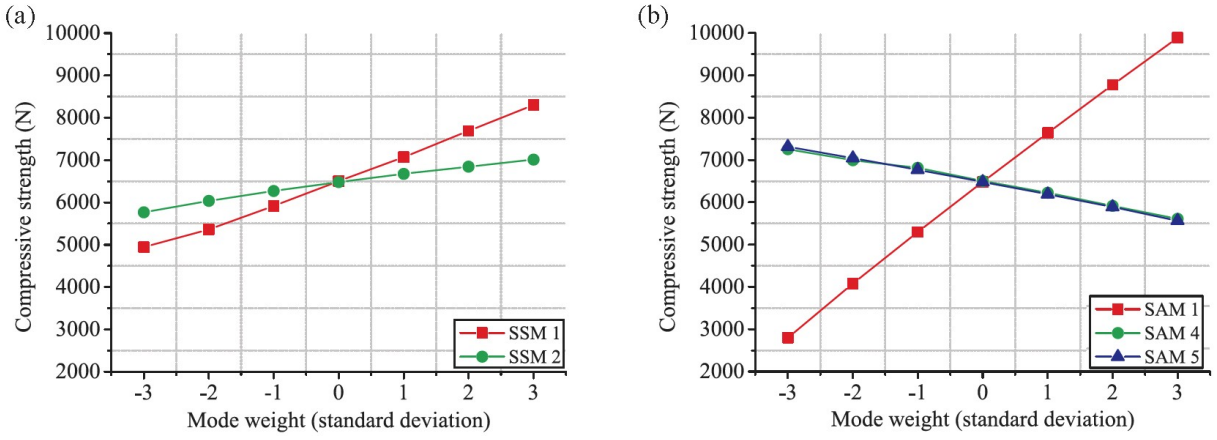


**Figure 8** Influences of shape and density distribution on compressive strength. (a) Influence of shape (SSM 1 and SSM 2) on compressive strength. (b) Influence of density distribution (SAM 1, SAM 4, and SAM 5) on compressive strength.

above independent analyses, it was indicated that the SAM modes contributed more to bone strength than the SSM modes, although the compactness of SAM was poor. Fully understanding the contributions of SSM and SAM modes to compressive strength has implications for optimizing MLR models to improve the accuracy and clinical utility for vertebral fracture assessment.

In addition to bone strength, our findings provided insight into the degeneration-related shape and density variations to fracture behavior. The major determinants (SSM 1 and SAM 1) of compressive strength were suggested to monitor fracture risk in degeneration processes. A one standard deviation decrease in SSM 1 was associated with a 550 N decrease in bone strength, and that in SAM 1 was associated with a 1200 N decrease. Vertebral strength could serve as a good predictor for assessing risk of bone fracture [41]. For example, the probability of the men aged 75 years at fragile bone strength (6500 N) was 14.80% [33]. Of note, SAM 1 exhibited great potential in the assessment of vertebral fracture patterns (Fig. 6). SAM 1 could describe the density distributions of degenerative vertebrae and quantify the locations with low densities, thus demonstrating the ability to recognize the regions with high strain. The positive SAM 1 represents relatively high-density bone, and the middle cross-section of vertebra tends to be the weakest area [36], leading to compression deformity. By contrast, the negative SAM 1 represents relatively low-density bone, the anterosuperior region of vertebral body cannot bear the applied load, and this situation might trigger deflection of the weakest cross-section, leading to wedge deformity. Taken together, SSM 1 and SAM 1 may help clinicians evaluate vertebral fracture risk and predict fracture locations.

There were several limitations to this study. First, the SSM and SAM of the L1 vertebrae were derived from an all-male dataset. Gender-related variations of shape and density distribution have been found in the vertebrae [6,42]. Therefore, statistical models would be re-constructed targeting the all-female or mixed-gender cohorts. Second, only the uniaxial compressive loading condition was simulated to calculate the strength of L1 vertebra. This is because this clinical relevant configuration is well-defined and repeatable [35], and it was proven to have a strong association with high fracture risk [33]. It should be noted that PC modes identified from the MLR analysis for bone strength under other loading configurations (e.g., lateral bending, forward flexion, etc.) may differ from those for compressive strength prediction. Finally, in our study, demographic information (e.g., age, height, weight, etc.) was not considered as the potential variable for developing MLR models. It was proven that demographic characteristics have only a minor contribution to the prediction of bone strength and related fracture risk [20].

## 5. Conclusions

In conclusion, the novelties of this study were that it quantitatively described the variations in shape and density distribution for the degenerated vertebrae with different degenerative states by using statistical models, identified the specific SSM/SAM modes to predict compressive strength, and quantified the effects of major modes on fracture behavior. These findings have great potential in different clinical applications, including disease diagnosis, fracture risk assessment, optimal implant design and selection, as well as preoperative planning for surgical treatments (such as lumbar fusion and disc replacement). In addition, this study may improve understanding of the pathological process of vertebra degeneration.

***Conflict of interest*** *On behalf of all authors, the corresponding author states that there is no conflict of interest.*

***Author contributions*** ***Meng Zhang:*** *Formal analysis, Investigation, Methodology, and Writing – original draft.* ***He Gong:*** *Conceptualization, Funding acquisition, Project administration, Supervision, and Writing – review & editing.* ***Ming Zhang:*** *Resources.*

***Acknowledgements*** *This work was supported by the National Natural Science Foundation of China (Grant No. 12272029).*

1 P. Khoddam-Khorasani, N. Arjmand, and A. Shirazi-Adl, Effect of changes in the lumbar posture in lifting on trunk muscle and spinal loads: A combined *in vivo*, musculoskeletal, and finite element model study, J. Biomech. **104**, 109728 (2020).
2 J. D. Auger, N. Frings, Y. Wu, A. G. Marty, and E. F. Morgan, Trabecular architecture and mechanical heterogeneity effects on vertebral body strength, Curr. Osteoporos. Rep. **18**, 716 (2020).
3 M. Millecamps, J. T. Czerminski, A. P. Mathieu, and L. S. Stone, Behavioral signs of axial low back pain and motor impairment correlate with the severity of intervertebral disc degeneration in a mouse model, Spine J. **15**, 2524 (2015).
4 J. F. M. Hollenbeck, C. M. Cain, J. A. Fattor, P. J. Rullkoetter, and P. J. Laz, Statistical shape modeling characterizes three-dimensional shape and alignment variability in the lumbar spine, J. Biomech. **69**, 146 (2018).
5 A. Valentinitsch, S. Trebeschi, E. Alarcón, T. Baum, J. Kaesmacher, C. Zimmer, C. Lorenz, and J. S. Kirschke, Regional analysis of age-related local bone loss in the spine of a healthy population using 3D voxel-based modeling, Bone **103**, 233 (2017).
6 Y. Masharawi, and K. Salame, Shape variation of the neural arch in the thoracic and lumbar spine: Characterization and relationship with the vertebral body shape, Clin. Anatomy **24**, 858 (2011).
7 S. H. Zhou, I. D. McCarthy, A. H. McGregor, R. R. H. Coombs, and S. P. F. Hughes, Geometrical dimensions of the lower lumbar vertebrae—analysis of data from digitised CT images, Eur. Spine J. **9**, 242 (2000).
8 A. Kanawati, R. J. R. Fernandes, A. Gee, J. Urquhart, F. Siddiqi, K. Gurr, C. Bailey, and P. Rasoulinejad, Geometric and volumetric relationship between human lumbar vertebra and CT-based models, Academic Radiol. **28**, e172 (2021).
9 M. Zhang, H. Gong, K. Zhang, and M. Zhang, Prediction of lumbar vertebral strength of elderly men based on quantitative computed tomography images using machine learning, Osteoporos. Int. **30**, 2271

(2019).
10 J. Kaiser, B. Allaire, P. M. Fein, D. Lu, A. Adams, D. P. Kiel, M. Jarraya, A. Guermazi, S. Demissie, E. J. Samelson, M. L. Bouxouxsein, and E. F. Morgan, Heterogeneity and spatial distribution of intravertebral trabecular bone mineral density in the lumbar spine is associated with prevalent vertebral fracture, J. Bone Mineral Res. **35**, 641 (2020).
11 A. Goparaju, K. Iyer, A. Bône, N. Hu, H. B. Henninger, A. E. Anderson, S. Durrleman, M. Jacxsens, A. Morris, I. Csecs, N. Mar-Marrouche, and S. Y. Elhabian, Benchmarking off-the-shelf statistical shape modeling tools in clinical applications, Med. Image Anal. **76**, 102271 (2022).
12 T. Liu, N. M. Jomha, S. Adeeb, M. El-Rich, and L. Westover, Investigation of the average shape and principal variations of the human talus bone using statistic shape model, Front. Bioeng. Biotechnol. **8**, (2020).
13 P. Soltanmohammadi, J. Elwell, V. Veeraraghavan, G. S. Athwal, and R. Willing, Investigating the effects of demographics on shoulder morphology and density using statistical shape and density modeling, J. Biomech. Eng. **142**, 121005 (2020).
14 L. Grassi, S. P. Väänänen, L. Jehpsson, Ö. Ljunggren, B. E. Rosengengren, M. K. Karlsson, and H. Isaksson, 3D finite element models reconstructed from 2D dual-energy X-ray absorptiometry (DXA) images improve hip fracture prediction compared to areal BMD in Osteoporotic Fractures in Men (MrOS) Sweden cohort, J. Bone Mineral Res. **38**, 1258 (2023).
15 M. Taylor, M. Viceconti, P. Bhattacharya, and X. Li, Finite element analysis informed variable selection for femoral fracture risk prediction, J. Mech. Behav. Biomed. Mater. **118**, 104434 (2021).
16 R. Bhalodia, S. Elhabian, J. Adams, W. Tao, L. Kavan, and R. Whi-Whitaker, DeepSSM: A blueprint for image-to-shape deep learning models, Med. Image Anal. **91**, 103034 (2024).
17 J. Pitocchi, R. Wirix-Speetjens, G. H. van Lenthe, and M. Á. Pérez, Integration of cortical thickness data in a statistical shape model of the scapula, Comput. Methods Biomech. Biomed. Eng. **23**, 642 (2020).
18 W. S. Burton Ii, I. Sintini, J. M. Chavarria, J. R. Brownhill, and P. J. Laz, Assessment of scapular morphology and bone quality with statistical models, Comput. Methods Biomech. Biomed. Eng. **22**, 341 (2019).
19 L. J. Ren, Y. Yu, Y. H. Zhang, X. D. Liu, Z. J. Sun, W. J. Yao, T. Y. Zhang, C. Wang, and C. L. Li, Three-dimensional finite element analysis on cochlear implantation electrode insertion, Biomech. Model. Mechanobiol. **22**, 467 (2023).
20 F. Jazinizadeh, J. D. Adachi, and C. E. Quenneville, Advanced 2D image processing technique to predict hip fracture risk in an older population based on single DXA scans, Osteoporos. Int. **31**, 1925 (2020).
21 F. Jazinizadeh, and C. E. Quenneville, Enhancing hip fracture risk prediction by statistical modeling and texture analysis on DXA images, Med. Eng. Phys. **78**, 14 (2020).
22 F. Jazinizadeh, and C. E. Quenneville, 3D analysis of the proximal femur compared to 2D analysis for hip fracture risk prediction in a clinical population, Ann. Biomed. Eng. **49**, 1222 (2021).
23 A. V. Pavlova, F. R. Saunders, S. G. Muthuri, J. S. Gregory, R. J. Barr, K. R. Martin, R. J. Hardy, R. Cooper, J. E. Adams, D. Kuh, and R. M. Aspden, Statistical shape modelling of hip and lumbar spine morphology and their relationship in the MRC national survey of health and development, J. Anat. **231**, 248 (2017).
24 S. Caprara, F. Carrillo, J. G. Snedeker, M. Farshad, and M. Senteler, Automated pipeline to generate anatomically accurate patient-specific biomechanical models of healthy and pathological FSUs, Front. Bioeng. Biotechnol. **9**, 636953 (2021).
25 N. C. Harvey, A. Odén, E. Orwoll, J. Lapidus, T. Kwok, M. K. Karlsson, B. E. Rosengren, Ö. Ljunggren, C. Cooper, E. McCloskey, J. A. Kanis, C. Ohlsson, D. Mellström, and H. Johansson, Falls predict fractures independently of FRAX probability: A meta-analysis of the Osteoporotic Fractures in Men (MrOS) study, J. Bone Mineral Res. **33**, 510 (2018).
26 H. J. Wilke, F. Rohlmann, C. Neidlinger-Wilke, K. Werner, L. Claes, and A. Kettler, Validity and interobserver agreement of a new radiographic grading system for intervertebral disc degeneration: Part I. Lumbar spine, Eur. Spine J. **15**, 720 (2006).
27 A. H. Gee, G. M. Treece, and K. E. S. Poole, How does the femoral cortex depend on bone shape? A methodology for the joint analysis of surface texture and shape, Med. Image Anal. **45**, 55 (2018).
28 B. G. Faber, D. Baird, C. L. Gregson, J. S. Gregory, R. J. Barr, R. M. Aspden, J. Lynch, M. C. Nevitt, N. E. Lane, E. Orwoll, and J. H. Tobias, DXA-derived hip shape is related to osteoarthritis: Findings from in the MrOS cohort, Osteoarthritis Cartilage **25**, 2031 (2017).
29 M. Peiffer, A. Burssens, K. Duquesne, M. Last, S. De Mits, J. Victor, and E. Audenaert, Personalised statistical modelling of soft tissue structures in the ankle, Comput. Methods Programs Biomed. **218**, 106701 (2022).
30 M. D. Ahrend, H. Noser, R. Shanmugam, F. Burr, L. Kamer, T. Kamarul, H. Hügli, A. Nagy, R. G. Richards, and B. Gueorguiev-Rüegg, Development of generic Asian pelvic bone models using CT-based 3D statistical modelling, J. Orthopaedic Translation **20**, 100 (2020).
31 H. Ziaeipoor, M. Taylor, and S. Martelli, Population-based bone strain during physical activity: A novel method demonstrated for the human femur, Ann Biomed Eng **48**, 1694 (2020).
32 K. Burkhart, B. Allaire, D. E. Anderson, D. Lee, T. M. Keaveny, and M. L. Bouxsein, Effects of long-duration spaceflight on vertebral strength and risk of spine fracture, J. Bone Mineral Res. **35**, 269 (2020).
33 D. L. Kopperdahl, T. Aspelund, P. F. Hoffmann, S. Sigurdsson, K. Siggeirsdottir, T. B. Harris, V. Gudnason, and T. M. Keaveny, Assessment of incident spine and hip fractures in women and men using finite element analysis of CT scans, J. Bone Mineral Res. **29**, 570 (2014).
34 M. Mirzaei, A. Zeinali, A. Razmjoo, and M. Nazemi, On prediction of the strength levels and failure patterns of human vertebrae using quantitative computed tomography (QCT)-based finite element method, J. Biomech. **42**, 1584 (2009).
35 S. L. Schoell, K. M. Beavers, D. P. Beavers, L. Lenchik, A. P. Marsh, W. J. Rejeski, J. D. Stitzel, and A. A. Weaver, Prediction of lumbar vertebral body compressive strength of overweight and obese older adults using morphed subject-specific finite-element models to evaluate the effects of weight loss, Aging Clin. Exp. Res. **31**, 491 (2019).
36 R. P. Crawford, C. E. Cann, and T. M. Keaveny, Finite element models predict in vitro vertebral body compressive strength better than quantitative computed tomography, Bone **33**, 744 (2003).
37 F. Johannesdottir, E. Thrall, J. Muller, T. M. Keaveny, D. L. Kop-Kopperdahl, and M. L. Bouxsein, Comparison of non-invasive assessments of strength of the proximal femur, Bone **105**, 93 (2017).
38 M. J. Silva, T. M. Keaveny, and W. C. Hayes, Computed tomography-based finite element analysis predicts failure loads and fracture patterns for vertebral sections, J. Orthopaedic Res. **16**, 300 (1998).
39 H. Qiu, H. Yang, Z. Yang, Q. Yao, S. Duan, J. Qin, and J. Zhu, The value of radiomics to predict abnormal bone mass in type 2 diabetes mellitus patients based on CT imaging for paravertebral muscles, Front. Endocrinol. **13**, 963246 (2022).
40 A. I. Hussein, T. M. Jackman, S. R. Morgan, G. D. Barest, and E. F. Morgan, The intravertebral distribution of bone density: Correspondence to intervertebral disc health and implications for vertebral

strength, Osteoporos. Int. **24**, 3021 (2013).
41 F. Song, Y. Wei, W. Feng, R. Fu, Z. Li, X. Gao, X. Cheng, and H. Yang, Biomechanical CT-computed bone strength predicts the risk of subsequent vertebral fracture, Bone **166**, 116601 (2023).
42 C. Chen, Y. Liu, S. Lee, H. Yang, and W. P. Chan, Gender interactions between vertebral bone mineral density and fat content in the elderly: Assessment using fat-water MRI, Magn. Reson. Imag. **51**, 1382 (2020).

# 通过量化形态和密度分布评估退变椎骨的强度及断裂行为

张萌, 宫赫, 张明

**摘要** 腰椎退行性病变可导致椎骨形状和密度分布发生改变, 进而影响其力学性能和行为. 本研究旨在通过统计形状模型(SSM)和统计外观模型(SAM)定量描述退变椎骨形状和密度分布的变化, 并利用特定主成分模式来评估椎骨的强度和断裂行为. 基于75名老年男性L1椎骨建立详细的SSM和SAM, 提取其主成分模式来定量描述退变椎骨形状和密度分布特征. 根据L1椎骨的退变程度, 将所有受试者分为轻度退变组($n$ = 22)、中度退变组($n$ = 29)和重度退变组($n$ = 24). 基于定量CT的有限元分析计算每个椎骨的抗压强度, 并利用多元线性回归分析来评估椎骨强度与主成分模式之间的关系. 对比分析SSM和SAM第一模式(平均值±3倍标准差)下等效塑性应变(PEEQ)的分布以评估退变椎骨的断裂模式. 留一法结果显示所建立的SSM和SAM具有良好的性能, 用它们对未知椎骨的形状和密度分布进行重建, 其平均绝对误差分别为0.335±0.084 mm和64.610±26.620 mg/cm$^3$. 使用4个主成分模式(SSM 1、SAM 1、SAM 4和SAM 5)构建的多元线性回归模型, 其强度预测性能良好. 此外, 与椎骨退变相关的形态变化相比, PEEQ的数值对密度分布的变化更为敏感. 椎骨密度分布的变化可能会影响其受力后的变形类型(压缩变形和楔形变形), 进而影响其骨折模式. 统计模型可以识别退变椎骨形状和密度分布的变化, 并且SSM/SAM模式可以用来评估椎骨的抗压强度和断裂行为. 上述研究结果对协助临床医生进行病理诊断、骨折风险评估、植入体的设计和术前规划具有重要意义.